



Future Climate Change Impact on the Streamflow of Mahi River Basin Under Different General Circulation Model Scenarios

Swati Maurya^{1,2} · Prashant K. Srivastava^{1,2} · Lu Zhuo³ · Aradhana Yaduvanshi⁴ · R. K. Mall²

Received: 1 July 2022 / Accepted: 21 October 2022
© The Author(s), under exclusive licence to Springer Nature B.V. 2023

Abstract

Climate change (precipitation and temperature) has significantly affected the hydrological regimes and future climate projection. Integration of climate model with physical based model is crucial for quantitative measurement of changes in surface water regime. For accurate estimation, modelling framework need finer scale resolution of climate model output. In this study, we examined the bias corrected, statistically downscale models drawn from the NASA, Earth Exchange Global Daily Downscaled Projections–Coupled Model Inter-comparison Project Phase 5 (NEX-GDDP-CMIP5) over the study region. The rainfall and temperature projection output from the INMCM-4, MRI-CGCM3 and their ensemble mean performed well over the Mahi River basin (MRB), India. In this study, the climate data integrated with the SWAT model to analyse the potential impact of climate change on the discharge of MRB. The finding indicates that in the near future (2011–2040) projection of annual average streamflow increases by 76.74% based on the INMCM-4 outputs, 25% based on the MRI-CGCM3 outputs, and 24.53% based on the ensemble mean in comparison to the baseline period (1981–2010). Further, the modelling results of mean monthly streamflow in rainy season indicated that the lowest and highest streamflow changes will be ranging from about 631.07–2718.42 m³/s as observed by INMCM-4, 491.71–2938 m³/s observed by MRI-CGCM3, 513.02–2270.18 m³/s observed by ensemble mean, in the near future. Similarly, in the summer season, the lowest level of stream flow is found to be 158.27 m³/s observed by MRI-CGCM3, 193.38 m³/s (ensemble mean) and 258.53 m³/s (INMCM-4), respectively. Additionally, the streamflow trend was assessed by Mann–Kendall and Sen's slope method at the monthly, seasonal and annual scales. The future streamflow projection represented the ascending trend observed in south west and winter monsoon, while the descending trend was observed in pre-monsoon and post-monsoon under the INMCM-4, MRI-CGCM3, and ensemble mean. Results on projected precipitation, temperature and streamflow accretion would help to develop effective adaptation measures for reducing the impacts of climate change and to work out long-term water resource management plans in the river basin.

Keywords SWAT · Climate change · Streamflow · NEX-GDDP-CMIP5, Future scenarios

Extended author information available on the last page of the article

1 Introduction

Water availability is an important criterion for deciphering the ecological, economic and geophysical level of a region (Barthel et al. 2010). The climate variation has a great impact on the trend and pattern of precipitation and temperature, which can significantly alter the hydrological processes of precipitation extreme, increasing evaporation and changing river runoff (Islam et al. 2012; Sabzevari et al. 2015) etc. These climate changes directly affect the hydrological system in several ways. Firstly, it can affect the water supplies in different fields, for instance, in agricultural, industrial and drinking purposes (Veijalainen et al. 2010). Secondly, natural hazards like floods and drought can impact the social lives of people and the economy of a nation (Ahsan et al. 2016). Therefore, the assessment of climate change impact is necessary for the hydrological regime of water resource development. In this context, downscaled GCMs climate models are an appropriate tool for understanding and evaluating climate change in the past and future. The downscaled GCMs output generates higher spatial resolution climate parameters by incorporating local topographic and physical factors, which make the GCMs more suitable for regional and local hydrological impact studies. Worldwide extensively application of downscaled GCMs (Narsimlu et al. 2013; Sunde et al. 2017; Bhatta et al. 2019; Bermúdez et al. 2020; Oo et al. 2020; Touseef et al. 2020; Ji et al. 2021) gain popularity due to accurate and reliable estimation of future earth climate scenarios. In this context, downscaled GCMs, including CMIP5 is better advanced to be used for hydrological modelling at the catchment level. The physical based hydrological model Soil and Water Assessment Tool (SWAT) has been extensively applied for evaluating the basin hydrology under different climate change scenarios at the global level. (Narsimlu et al. 2015; Uniyal et al. 2015) Examine the impact of climate change on water balance of the Baitarani river basin using SWAT model results suggested that surface runoff ranged from 2.5 to 11% by changing the temperature from 1 to 5 °C, whereas the increase in rainfall by 2.5 to 15% from the baseline condition.

Recently, NASA has launched the NEX-GDDP datasets, downscaled climate scenarios from the Coupled Model Intercomparison Project Phase 5 (CMIP5) (Raghavan et al. 2018). The data has been statistically bias-corrected and has a high spatial resolution of $0.25^{\circ} \times 0.25^{\circ}$ and is available in daily time steps, which has been proven to be a promising source of climate projection at both regional and local scales (Sarathi et al. 2015; Parth Sarathi et al. 2016; Raghavan et al. 2018; Sahany et al. 2019; Kumar et al. 2020). For example (Usman et al. 2021) applied NEX-GDDP inputs to simulate the hydrological model under the historical and future scenarios (under the RCP 4.5 and RCP 8.5 emission scenarios). The results reported that projected streamflow decreased significantly over the Son river basin. (Li et al. 2020) assessed NEXGDDP datasets to predict future runoff and flood risk by using the SWAT model. The forecast result indicated that the return period of extreme runoff will increase by 10%~25% under the eight climate models in 2050. Similarly, (Xu et al. 2021) reported the average annual precipitation and the average annual temperature would both increase, but the mean annual streamflow would decrease during 2021–2050, over the Amu Darya River Basin. (Musie et al. 2020) compared the CORDEX-AFRICA and NEX-GDDP data over the Lake Ziway sub-basin, Ethiopia. The analysis indicated that all the climate model of NEX-GDDP are not well performed over the region. While the annual average streamflow of CORDEX-AFRICA dataset, is expected to increase towards the end of the century under both climate scenarios (RCP4.5 and 8.5). (Jain et al. 2019) also evaluated the 1975–2005 daily data of NEX-GDDP using the India Meteorological Department observations and compared the dataset with CMIP5

and CORDEX data over India. They also supported the use of NEX-GDDP datasets for regional-scale climate change impact studies. To this end, an integrated approach of high-resolution climate change scenarios with the hydrological models will provide useful insights for impact assessment in terms of the quantity of the water resource.

Therefore, the main aims of this study are to understand how future climate will alter the streamflow of the Mahi River Basin (MRB) that can be achieved by the following objectives: The first objective is to evaluate the performance of the six models namely; GFDL-CM3, INMCM-4, MPI-ESM-LR, MRI-CGCM3, CanESM2, GFDL-ESM2M and ensemble mean of the NEX-GDDP-CMIP5 with observed datasets. The second objective is to forecast the future average monthly and annual streamflow coupled with the SWAT model. In Gujarat, MRB is the largest west flowing perennial river with great ecological, economic, religious, and aesthetic significance. Further, MRB is the principal source of water supply for drinking, agricultural and industrial etc. uses. Several studies have been conducted (Sridhar 2009; Sahu et al. 2016; Pawar and Hire 2018; Bhati et al. 2021; Das and Scaringi 2021), which the main focus on rejuvenating and sustaining the basin, strengthening the agricultural economy and livelihood etc. Unfortunately, no previous study was reported to examine the climate change on the river's streamflow. Thus, this innovative study quantifies the importance of the SWAT model for the prediction of riverine streamflow under a future climate using new bias-corrected and finer-resolution climate datasets of NEX-GDDP-CMIP5.

2 Study Area

Mahi River is an inter-state (Rajasthan, Gujarat and Madhya Pradesh) perennial river of India. It is the longest west flowing river that originates at the northern slope of the Vindhyan mountain range, Dhar district of Madhya Pradesh and drains into the Gulf of Khambhat, as shown in Fig. 1. The topography of all the states differs from one another. Part of Rajasthan

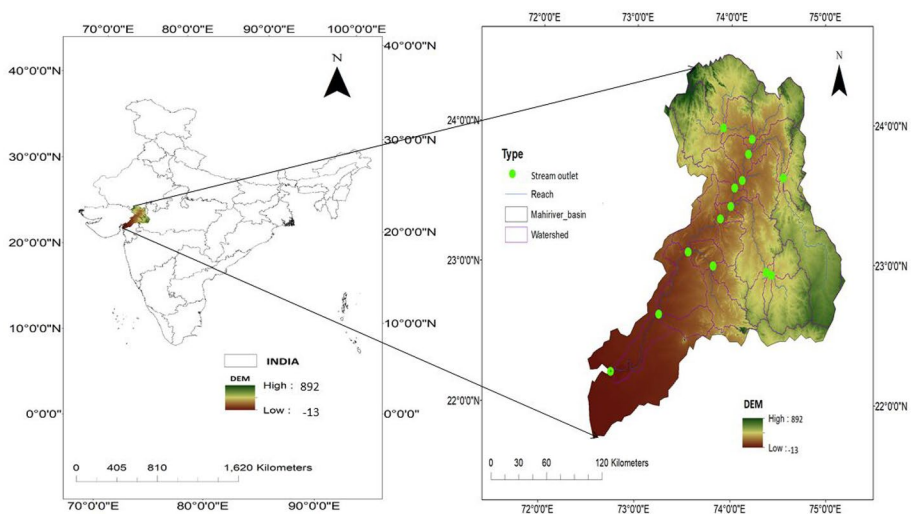


Fig. 1 Geographical location of the study area

comprises hills, forests and eroded terrain, while Gujarat has flat, fertile land. Madhya Pradesh has undulating land with ridges and plain area. The changing topography through which the Mahi River flows has a huge ecological and economic significance. The total length of the basin is 583 km, and the drainage area is approx. 34,842 sq km. Approximately 63.63% of the catchment area around the basin is covered by agricultural land, 19.29% by forest, while the rest comprises water bodies. The basin falls under two climatic conditions, namely, sub-tropical and tropical wet. The temperature of the basin varies from 3 to 47 °C.

3 Materials and Methods

3.1 NEX-GDDP-CMIP5 Datasets

The high-resolution dataset generated from the NEX-GDDP-CMIP5 have been adopted in this study. This dataset has facilitated the study of climate variability and its impact on past and future climate at regional scales. NEX-GDDP uses a statistically downscaling algorithm called the Bias-Correction Spatial Disaggregation (BCSD) method to overcome the limitation of GCMs projections. The BCSD method is categorised into two parts for the period 1950–2005 of the CMIP5 historical runs. The first part involved correcting the bias of the GCMs by using simple statistical measures of the mean, variances, slope etc., compared with the observed datasets of the Global Meteorological Forcing Datasets (GMFD) available from the Terrestrial Hydrology Research Group from Princeton University. The second part involved spatial disaggregation, which interpolates the coarse resolution of GCM data into finer resolution ($0.25^0 \times 0.25^0$) through the observed datasets. The NEX-GDDP provides the set of three climatic variables, including daily maximum temperature, minimum temperature, and precipitation for the Retrospective Run (1950–2005) and the Prospective Run (2006–2100) with the two projections as RCP 4.5 and RCP 8.5 from the 21 CMIP5 GCMs.

The NEX-GDDP-CMIP5 dataset is archived at <https://cds.nccs.nasa.gov/nex-gddp/>. This study mainly focuses on the climate projection of 20th-century experiments (RCP 4.5 scenario is extensively used RCP scenario in climate projections studies (Yaduvanshi et al. 2021), and the radiative forcing doesn't rise continuously like RCP 8.5). Our time period of projected streamflow is till 2030; therefore, we chose RCP 4.5 scenario. Six models, namely; GFDL-CM3, INMCM-4, MPI-ESM-LR, MRI-CGCM3, CanESM2, GFDL-ESM2M are selected from the NEX-GDDP-CMIP5, which is based on their performance as presented in previous studies in India (Chaturvedi et al. 2012; Mishra et al. 2014; Basha et al. 2017).

3.2 SWAT Model

The SWAT model is a physically-based, semi-distributed hydrological model used to assess the land management practices in water, sediment, agriculture of a large watershed along with various types of soil, land use and management practices for long periods of time (Arnold and Allen 1996). Based on the set of soil types, land use and slope, the catchment is divided into sub-basins which are further subdivided into the smallest sub-unit, such as; hydrological response units (HRUs) (Arnold et al. 1998).

Its working principle follows the water balance equation as;

$$SW_t = SW_o + \sum_{i=1}^n (R_{day} - Q_{surf} - E_a - W_{seep} - Q_{gw}) \quad (1)$$

where SW_t represents the final soil water content, SW_o represents the initial soil water content, R_{day} represents the amount of precipitation, Q_{surf} represents the amount of surface runoff, E_a represents the amount of Evapotranspiration, W_{seep} represents the amount of percolation and bypass exiting the soil profile bottom, Q_{gw} represents the amount of return flow.

In SWAT, the surface runoff is calculated by Soil Conservation Service Curve Number (SCS curve number). Here SCS curve numbers are estimated by the following equation;

$$Q_{surf} = \frac{(R_{day} - 0.2S)^2}{(R_{day} + 0.8S)} \quad (2)$$

$$R > 0.2S$$

where, Q_{surf} is the accumulated run-off or rainfall excess (mm), R_{day} is the rainfall depth for the day (mm) and S is a retention parameter (mm).

Runoff will occur when $R_{day} > 0.2S$. The retention parameter varies accordingly to the soil, land use, management practices and slope pattern. The retention parameter is represented as:

$$S = 25.4 \left(\frac{1000}{CN} - 10 \right) \quad (3)$$

where, CN is the curve number for the day.

3.3 SWAT Model Input Datasets

To run the SWAT model, the main input files are the Digital Elevation Model (DEM), soil types, land use and land cover, and hydrometeorological datasets. All the datasets are listed in Table 1.

3.3.1 Digital Elevation Model (DEM), Land Use and Soil Types

DEM is the primary component for SWAT model simulation for defining watershed boundary and delineated into sub-watersheds according to their elevation. Additionally, various types of parameters e.g., stream network, slope, aspect and channel width, etc. are extracted by 30 m DEM in this study Fig. 2a.

The Land use Land cover (LULC) map is accessed from the Global Land Cover Characterization database (GLCC) of the U.S. Geological Survey, which has a spatial resolution of 1 km (Bird et al. 2008). The LULC has approx. 83.10% area covered by cropland, 4.06% by forest area and 12.84% area covered by water, urban, wetland, and grassland, as shown in Fig. 2b.

The soil maps of this study are accessed from the Food and Agriculture Organization (FAO) United Nations, global soil data at 1 km resolution. This data provides information on the physio-chemical properties of soil, such as water storage limit, organic content, bulk density, clay, silt and sand fraction at the depth 0–30 cm (topsoil) and 30–100 cm (subsoil) of each soil types. The primary six different types of soil groups are cambisols (12.18%),

Table 1 A list of datasets used for Mahi River Basin

No	Spatial data	Description	Source
1.	Digital Elevation Model (DEM)	30 m x 30 m grid	Shuttle Radar Topography Mission of USGS http://srtm.csi.cgiar.org/
2.	Land use and Land cover (LULC)	1 km resolution	Global Land Cover Characterization (GLCC) database of the United state Geological survey https://earthexplorer.usgs.gov/
3.	Soil data	1:5000,000	Food and Agricultural Organization (FAO) http://gisserver.civil.iitd.ac.in/grbmp/
4.	Weather data	Relative humidity, solar radiation, wind speed (0.5 degree) Precipitation (1 degree), Temperature (0.25 degree) Streamflow data (cumsec)	National Center for Environment protection (NCEP) http://globalweather.tmu.edu/ Indian Meteorological Department (IMD), Pune
5.	Hydrological data		Central Water Commission (CWC), Gujarat

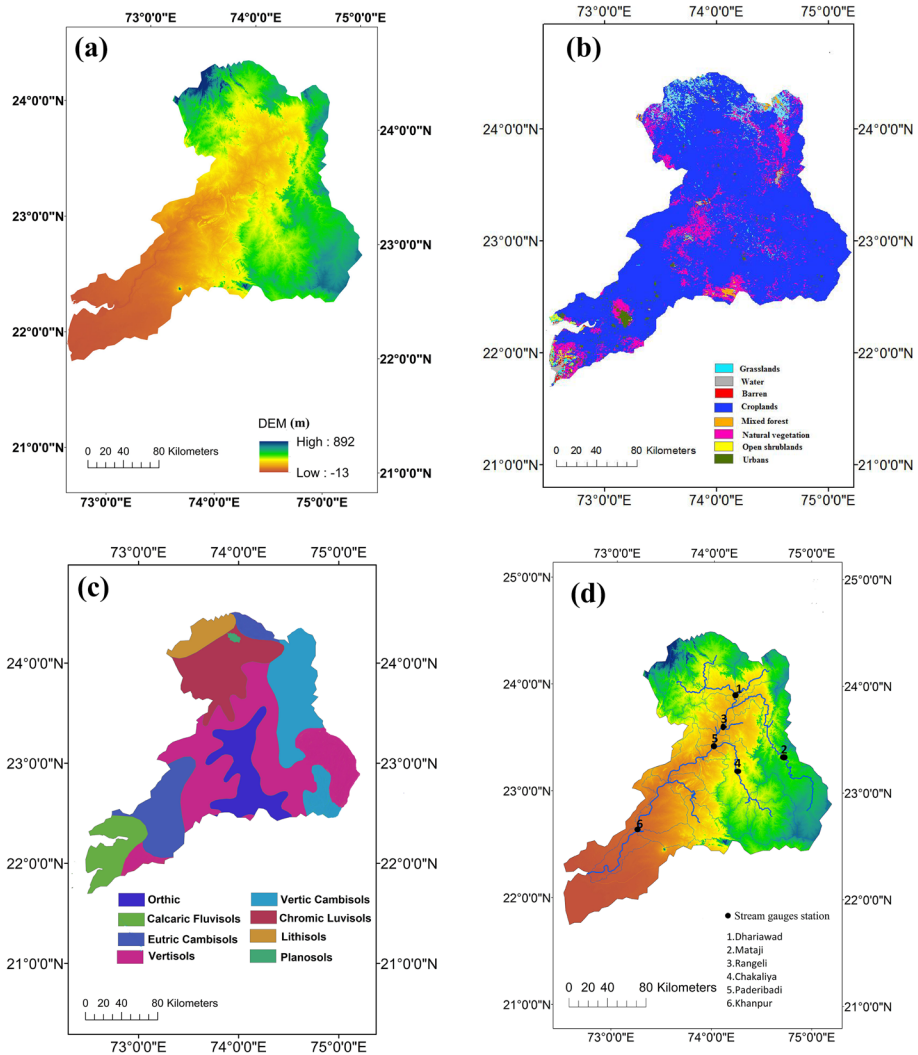


Fig. 2 a Digital elevation model; b Land use and land cover; c Soil types; d and Stream gauges station of the study area

lithosol (3.85%), vertisols (49.25%), luvisols (13.80%), acrisols (10.66%), and fluvisols (6.88%) shown in Fig. 2c.

3.3.2 Hydrometeorological Datasets

The Indian Meteorological Department (IMD) gridded rainfall datasets at $0.25^0 \times 0.25^0$, and maximum and minimum temperatures at $1^0 \times 1^0$ are available over the Indian region. The IMD uses the highest number of 6955 rain gauge stations to have a combination of hydro-meteorology, agromet observatory stations to estimate the accurate rainfall at a daily

scale (Pai et al. 2014). The gridded data was obtained from the rain gauge stations, and quality was improved by various information such as; coding and typo error correction, extreme values, etc. IMD uses Inverse Distance Weighted (IDW) interpolation technique along with the radial distance to convert the gauge stations data into gridded data. In this study, data from 1981–2012 rainfall, maximum and minimum temperature are taken from the six meteorological stations over the Mahi river basin Fig. 2d.

The relative humidity, wind speed, and solar radiation datasets are acquired from the National Centres for Environmental Prediction (NCEP), Climate Forest System Reanalysis (CFSR) during the period from 1998–2012. The NCEP-CFSR weather is estimated by cutting-edge data-assimilation techniques by using meteorological gauge station observations and satellite irradiances inclusive of atmospheric, oceanic, and surface-modelling components available at 0.5 degree resolution (Saha et al. 2010).

3.3.3 Streamflow Datasets

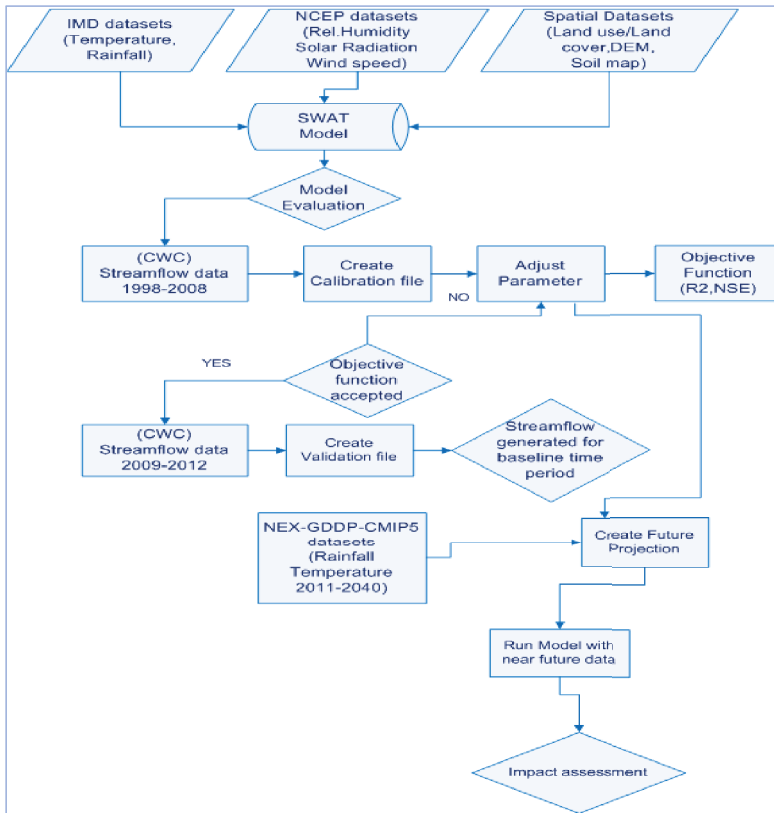
The Central Water Commission Committee of the Ministry of Water Resource Government of India installed a number of streamflow gauge stations in the tributaries of river basins across India for hydrological studies. The streamflow is measured at the gauge station once at time 08:00 h daily by the area-velocity method. The daily streamflow data from 1998–2012 was taken from the Central Water Commission (CWC) Gujarat at a daily time step for the six stream gauge stations, as shown in Fig. 2d.

3.4 Methodology

The primary goal of this research is to assess the impact of future climate variables on the river's hydrologic system. Figure 3 depicts the methodology framework of this study, which includes (i) prepared the spatial datasets and climate variables into SWAT format, (ii) model setup, including watershed delineated into sub-watersheds and Hydrologic Response Units (HRUs), (iii) calibration and validation of the model, and (iv) Future climate change impacts on streamflow are being assessed. ArcSWAT version 10.1, an ArcGIS extension-based SWAT model has been used in this study. SWAT is a physical based model that needed a digital elevation model (DEM), a land use and soil map, and daily weather data as primary input datasets. The SWAT-CUP programme is used for calibration and validation. Several hydrological model parameters are adjusted at this stage to accomplish the best suitable between the simulated and measured flow at the monitoring station. Finally, the climate change impact on the future streamflow is projected using the model.

3.4.1 SWAT Model Simulation

The SWAT model was simulated for approx.15 years. The time frame taken for this study is 1998–2012, from which 1998–2000 (warm-up period) are used to initiate the model's state variables and (2001–2008) are utilized for calibration. The validation period is up to 4 years approx. from 2009 to 2012. After the proper calibration and validation of the SWAT model, it is used to simulate the streamflow in the MRB during the baseline (1981–2010) and near future (2011–2040) time series to calculate the climate change impact. The future hydrological conditions are simulated using the downscaled precipitation and temperature dataset of the NEX-GDDP-CMIP5.



*NCEP, National Centers for Environmental Prediction; IMD, Indian Meteorological Department; CWC, Central Water Commission;

Fig. 3 Schematization of the Methodology

3.5 Calibration and Uncertainty Analysis Techniques

3.5.1 Sequential Uncertainty Fitting Version-2 (SUFI-2)

Bayesian framework-based SUFI-2 method estimates uncertainties by using the sequential and fitting process. SUFI-2 accounts for all types of uncertainties, for example, input, structural, parameter and response uncertainty. A combination of optimization and global uncertainty analysis is applied through the Latin Hypercube Sampling (Abbaspour et al. 2007). However, output uncertainty is measured by the 95% prediction uncertainty band (95PPU) examined by the 2.5% and 97.5% levels of the cumulative distribution function of the output variables (Abbaspour et al. 2004). The process of the SUFI-2 is described below;

1. Firstly, the objective function (θ) and meaningful parameter ranges [$\theta_{\text{abs min}}$, $\theta_{\text{abs max}}$] are calculated. After that, the Latin Hypercube sampling approach is applied to evaluating the objective functions, and the given formula computes the sensitivity matrix J and the parameter covariance matrix C

$$J_{ij} = \frac{\Delta g_i}{\Delta \theta_j}, \quad i = 1, \dots, C_2^m, \quad j = 1, \dots, n \quad (4)$$

$$C = S_g^2 (J^T J)^{-1} \quad (5)$$

where, S_g^2 is the variance of the objective function values resulting from the m model runs.

2. A 95% predictive interval of a parameter θ_j is computed as follows;

$$\theta_{j,\text{lower}} = \theta_j^* - t_{v,0.025} \sqrt{c_{jj}}, \quad \theta_{j,\text{upper}} = \theta_j^* + t_{v,0.025} \sqrt{c_{jj}} \quad (6)$$

where θ_j^* is the parameter θ_j for the best estimates (i.e. parameters which produce the optimal objective function), and v is the degree of freedom ($m-n$).

3. The two indices, such as the p-factor (the percent of observations bracketed by the 95PPU) and the r-factor are calculated. After which 95PPU is calculated

$$r\text{-factor} = \frac{\frac{1}{n} \sum_{i=1}^n (y_{t,97.5\%}^M - y_{t,2.5\%}^M)}{\sigma_{obs}} \quad (7)$$

where $y_{t,97.5\%}^M$ and $y_{t,2.5\%}^M$ represent the upper and lower boundary of the 95PPU, and σ_{obs} stands for the standard deviation of the measured data.

The effectiveness of the calibration and uncertainty of the SWAT model performance is judged by the p-factor and r-factor. The p-factor represents the percentage of the measured data bracketed at the 95PPU, and when the value is close to 1, it is 100% (Abbaspour et al. 2004). The value of the r-factor is the ratio of average thickness of the 95PPU to the standard deviation of the measured data. The lesser value of r-factor indicates less uncertainty, while a value close to 1 indicates higher uncertainty.

4 Performance Indices

4.1. The Nash–Sutcliffe coefficient (NSE) and Coefficients of determination (R^2) are used as goodness-of-fit indicators for the evaluation of the SWAT model due to its flexibility. The value of NSE varies from $-\infty$ to 1, where 1 indicates 100% correct simulation of the model, and negative values indicate that the mean observed value is over predicted to the simulated values (Nash and Sutcliffe 1970). It describes how well the plot fits 1:1 line between observed and simulated data. NSE is calculated as

$$NSE = 1 - \frac{\sum_{i=1}^n (Q_m - Q_s)_i^2}{\sum_{i=1}^n (Q_{m,i} - \bar{Q}_m)^2} \quad (8)$$

where, Q_m is the mean of observed streamflow, and Q_s is the simulated streamflow and n is the total number of observations.

4.2 R^2 defines the proportion of the total variance. Its range varies from 0 to 1, where a higher value indicates good performance (Kumar et al. 2017). R^2 is calculated as

$$R^2 = \frac{\left[\sum_i (Q_{m,i} - \bar{Q}_m)(Q_{s,i} - \bar{Q}_s) \right]^2}{\sum_i (Q_{m,i} - \bar{Q}_m)^2 \sum_i (Q_{s,i} - \bar{Q}_s)^2} \quad (9)$$

where, Q for streamflow, m and s for measured and simulated values, respectively.

5 Results and Discussion

5.1 SWAT Model Performance and Evaluation

5.1.1 Sensitivity Analysis

SWAT-CUP (calibration and uncertainty programs) interface has been used for sensitivity, calibration and uncertainty analysis of model. In SWAT-CUP, a large number of model parameters are given, such as sediment yield, water quality, streamflow, soil nutrient etc., which are determined by relevant articles carried out in basins with similar environmental conditions (Santhi et al. 2001; Lenhart et al. 2002). The seventeen parameters which are important for the model performance are CN2, ALPHA BF, GWDELAY, GWQMN, REVAPMN, ESCO, CH N2, CH K2, ALPHA BNK, SOL AWC, SOL K, SOL BD, OVN, SLSUB BSN, SFTMP and HRU SLP. After identifying sensitive parameters in SWAT CUP, some parameters are adjusted by default, and some parameters range are further adjusted and calibrated in the model for better streamflow results. The t-stat and p-value help in the identification of the most sensitive parameters among the seventeen parameters. The larger value of t-stat and the smaller value of p indicate the most sensitive parameters, which are shown in Table 2.

The most sensitive parameters of the MRB are curve number (CN2), alpha factor for bank storage (ALPHA BNK) and groundwater revap coefficient (GW REVAP). These parameters were also found sensitive by other researchers as in (Thampi et al. 2010).

5.1.2 Calibration, Uncertainty Analysis and Validation

Calibration and uncertainty analysis are applied to parameterize a model to minimize the predictive uncertainty and the difference between the model simulation and observation. 1000 simulations are applied to gain a better estimation of the streamflow to calibrate the model for the period 2001–2008 (Fig. 4a). Further, the model performance is tested by objective functions NSE, R^2 , p-factor and r-factor. The dotted plot is the plot of a parameter value corresponding to the objective function (NSE) analysed, as shown in Fig. 5. The parameter sensitivity is expressed by the scattering of sampling points i.e., random and dispersed points suggested that the sensitivity is low. And a certain pattern is liked to be sensitivity is higher. The minimum value of NSE 0.5 (threshold value for behavioral) is considered in this study (Yaduvanshi

Table 2 The range of sensitive parameters of SUFL-2 in the calibration

No	Parameters	Description	t-stat	p-value	Fittedvalue	Min value	Max value
1.	r_OV_N.hru	Manning's n value for overland flow	-0.36	0.71	-0.09	-0.20	0.00
2.	r_SLSUBBSN.hru	Average slope Length (m)	0.18	0.85	9.06	5.00	10.00
3.	v_ESCO.hru	Soil evaporation Compensation factor	-3.48	0.05	0.80	0.80	1.00
4.	v_CH_N2.rte	Manning's n value for the main channel	0.31	0.75	0.13	0.00	0.30
5.	v_GW_REVAP.gw	Ground water revap coefficient	1.66	0.09	0.14	0.00	0.30
6.	r_HRU_SLP.hru	Average slope Steepness(m/m)	0.73	0.46	0.18	0.00	0.20
7.	v_CH_K2.rte	Effective hydraulic conductivity	-4.34	0.01	28.18	5.00	130.0
8.	v_ALPHA_BF.gw	Base flow alpha factor	0.23	0.81	0.18	0.0	01.0
9.	r_SOL_K(...).sol	Saturated hydraulic	1.41	0.15	0.36	-0.80	0.80
10.	v_SFTMP.bsn	Snowfall temperature	0.60	0.95	-1.47	-5.00	5.00
11.	r_SOL_AWC(...).sol	Available water capacity	-0.54	0.58	0.29	-0.04	0.04
12.	r_SOL_BD(...).sol	Moist bulk density	-0.38	0.69	0.42	-0.50	0.60
13.	v_GW_DELAY.gw	Ground water delay	1.03	0.30	22.06	0.00	1.00
14.	v_ALPHA_BNK.rte	Bank flow recession	4.24	0.20	0.98	0.00	1.00
15.	r_CN2.mgt	Curve number II	-40.78	0.00	-0.18	-0.20	0.20
16.	v_GWQMN.gw	Threshold water depth of water in the shallow aquifer for return flow	0.94	0.34	11.5	0.00	100.00
17.	v_REVAPMN.gw	Threshold depth of water in the shallow aquifer for revap to occur (mm H ₂ O)	1.66	0.09	5.7	30.00	10.0

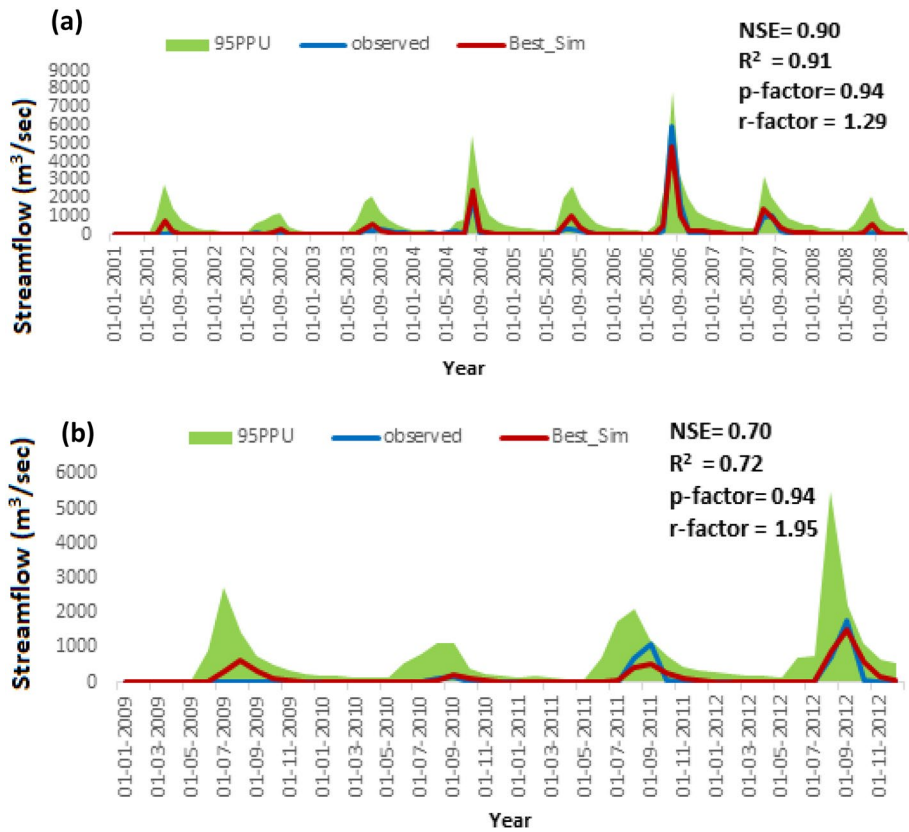


Fig. 4 **a** 95PPU plot derived by SUFI-2 method during calibration period from (2001–2008). **b** 95PPU plot derived by SUFI-2 method during validation period from (2009–2012)

et al. 2018). During the calibration process, the prediction uncertainty (95PPU) against the observed streamflow using the SUFI-2 technique is expressed in Fig. 4a. 95PPU depicts the uncertainty of the model and well captures the peak of the streamflow from January 2001 to December 2008. The r-factor (0.89) and p-factor (0.94) are obtained, respectively. The high value of NSE (0.91) and R^2 (0.92) indicates that the model performed well.

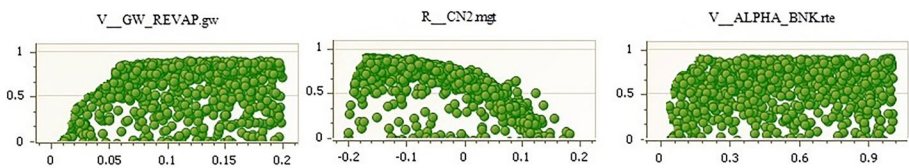


Fig. 5 Dotty plots with the objective function of NSE coefficient against each aggregate SWAT parameter. x-axis with sensitive parameters and y-axis as NSE

Further, the validation process is done using observed streamflow data (1000 times run) for the period 2009–2012. The value of evaluation statistical measures such as R^2 (0.72), NSE (0.70) and p-factor (0.94), r-factor (1.95) are obtained respectively (Fig. 4b). The high value of R^2 , NSE, p-factor and r-factor in the calibration and validation process fulfil the criteria of model performance (Moriassi et al. 2015) and results depict that the calibrated model performs well and can simulate the streamflow for future projection. Therefore, the calibrated model is used to examine the potential impacts of climate change on the water resource developer of the MRB.

5.2 Model Evaluation

The performance of the annual mean of rainfall and temperature dataset of the six models and their ensemble mean (average of the multiple models) of the NEX-GDDP-CMIP5 and IMD (observed) during the baseline time period (1981–2010) is depicted using the Taylor diagram as shown in Fig. 6a–c. The Taylor diagram of rainfall concludes that the individual model and ensemble mean cluster lies between the correlation coefficient of 0.9 to 0.99. However, the standard deviation value of the MRI-CGCM3, INMCM-4 and ensemble mean is close to 0.75 mm/day with a Root Mean Square (RMS) value of approximately 0.075 mm/day. Compared with the ensemble mean, INMCM-4 and MRI-CGCM3 have slightly higher RMS (0.18 and 0.13 mm/day). Thus overall analysis suggested that the INMCM-4, MRI-CGCM3 and ensemble mean performed better than other models and can be used for future climate change projection (Fig. 6a). We had already assessed the precipitation data of six models of NEX-GDDP-CMIP5 over the MRB for a baseline period 1981–2010, with detailed description provided in a previous paper (Maurya et al. 2021). In continuation to previous work, we have also assessed the maximum and minimum temperature data of six models of NEX-GDDP-CMIP5 with the observed datasets during the baseline period.

Figure 6b, c, indicate a successful performance for the maximum and minimum temperature variable by all the individual model and ensemble mean of NEX-GDDP-CMIP5. However, all individual models and ensemble mean have the highest correlation of 0.99 and a low error (RMS) of approximately to 0 and a standard deviation value close to 1. Further, the overall analysis suggests that precipitation projections are more uncertain with large variability than temperature projection.

5.3 Climate Change Scenario Generation

The scenarios of future climate are calculated by the differences (temperature) and percentage change (rainfall) in the near future (2011–2040) relative to the baseline time series (1981–2010), as shown in Tables 3 and 4. This analysis aims to observe the performance of these downscaled NEX-GDDP-CMIP5 model in order to evaluate the streamflow in the near future (2011–2040). Rainfall percentage (Table 3) indicates that rainfall decreases in the month of June, July and increases in the month of August and September of INMCM-4, MRI-CGCM3 and ensemble mean, respectively. This implies that under this scenario, rainfall may be slightly shifted in August and September, which would be beneficial for the agricultural field. From Table 4, it reveals that the maximum and the minimum temperature in the near future (2011–2040) increases in all months of the INMCM-4, MRI-CGCM3 and ensemble mean.

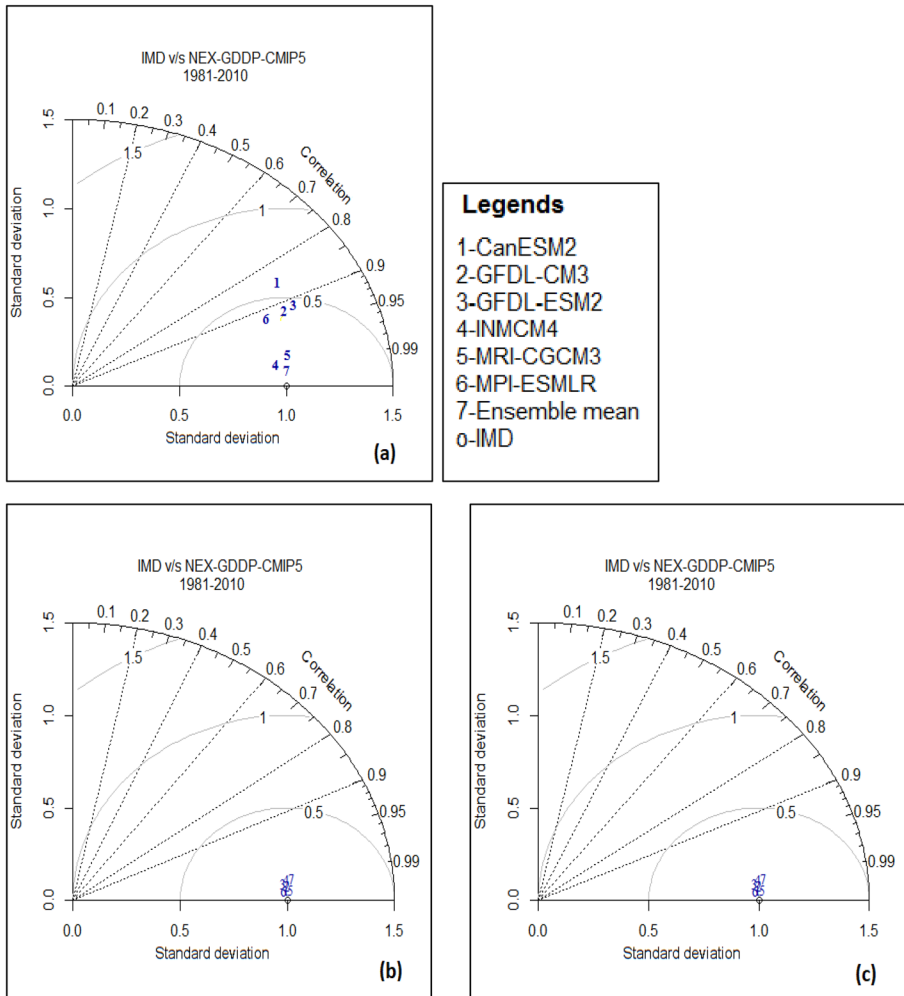


Fig. 6 Taylor diagram of NEX-GDDP-CMIP5 models versus IMD annual mean of **a** Rainfall **b** Maximum temperature, and **c** Minimum temperature during the period 1981–2010

Figures 7 and 8a–b depict the box-whisker plot of annual average rainfall, maximum and minimum temperature of the INMCM-4, the MRI-CGCM3 and the ensemble mean. The box-whisker plots provide information about the spread and skewness observed in

Table 3 Average monthly rainfall changes for (2011–2040) with respect to (1981–2010), percent change (%)

Month	Ensemble	INMCM-4	MRI-CGCM3
June	–8.45	–7.97	–6.21
July	–8.20	–7.75	–6.96
August	18.17	16.10	12.30
September	9.77	4.37	7.91

Table 4 Average monthly maximum and minimum temperature ($^{\circ}\text{C}$) changes for (2011–2040) with respect to (1981–2010) (2011–2040)

Month	Tmax			Tmin		
	Ensemble	INMCM-4	MRI-CGCM3	Ensemble	INMCM-4	MRI-CGCM3
Jan	1.62	1.57	1.47	1.80	1.94	1.86
Feb	1.72	1.96	1.87	1.35	1.43	1.74
March	1.50	1.54	1.61	1.26	1.13	0.98
April	1.71	1.85	1.79	1.46	1.29	1.67
May	2.39	1.91	2.01	1.77	1.96	2.02
June	2.33	2.68	2.58	1.93	1.75	1.85
July	1.94	1.89	1.86	1.83	1.69	1.43
August	2.49	2.01	2.55	2.26	1.98	2.21
Sep	1.83	1.73	1.69	1.99	1.75	1.43
Oct	1.49	1.33	1.53	2.29	1.84	2.21
Nov	1.70	1.65	1.59	2.05	2.01	2.12
Dec	1.42	1.37	1.49	1.74	1.69	1.58

the datasets, specifically, the upper quartile, the median line (centre) and the lower quartile. The whiskers represent a dotted line at each end of the box through the minimum and maximum values, and hollow circles show the outliers. Figure 7 shows that rainfall of the INMCM-4 and MRI-CGCM3 has higher variability than the ensemble mean, and no fixed pattern (continuously increasing or decreasing) has been observed in comparison to IMD data. While, the maximum and minimum temperature of INMCM-4, MRI-CGCM3 and ensemble mean have lesser variability and a continuous increasing pattern has been observed as compared to IMD, Fig. 8a and b.

5.4 Streamflow Projection Under Future Climate Scenario

The future climate datasets of INMCM-4, MRI-CGCM3 and ensemble mean have been used as input in the SWAT model for streamflow prediction. The mean annual streamflow of the baseline time series (1981–2010) is found to be $583.45 \text{ m}^3/\text{sec}$. In the near future (2011–2040), the high value of the projected mean annual streamflow is observed as $1031.24 \text{ m}^3/\text{sec}$ from the INMCM-4, and the low value of the mean annual streamflow is observed as $778.71 \text{ m}^3/\text{sec}$ from the MRI-CGCM3, and the mean annual streamflow is observed as $773.11 \text{ m}^3/\text{sec}$ from the ensemble mean. The streamflow at 95PPU

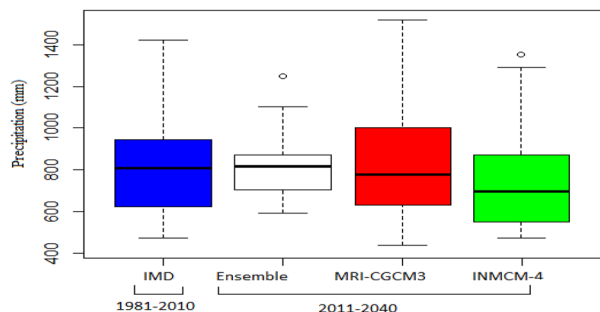
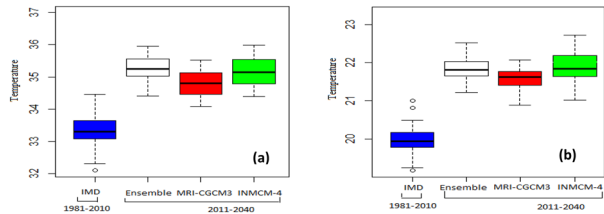
Fig. 7 Box-Whisker plot of annual average rainfall of NEX-GDDP-CMIP5 v/s IMD datasets

Fig. 8 Box-Whisker plot of the annual average of **a** Maximum temperature ($^{\circ}\text{C}$) **b** Minimum temperature ($^{\circ}\text{C}$) of NEX-GDDP-CMIP5 v/s IMD datasets



(95% prediction uncertainty) of INMCM-4, MRI-CGCM3 and ensemble mean model in the near future time series 2011–2040 is shown in Fig. 9a–c. The results depict that the higher streamflow approx. 10000 m^3/sec was observed in the year 2028 (INMCM-4) while approx 8000 m^3/sec was observed in the year 2027 (MRI-CGCM3), 2035 (ensemble mean), and 2033 (INMCM-4). However, it is interesting to notice that the streamflow of approx. 3000–4000 m^3/sec is observed throughout the year by MRI-CGCM3, INMCM-4, and ensemble mean.

Further, the distribution of monthly streamflow over the 30 years (2011–2040) is plotted with the baseline period (1981–2010) streamflow, as shown in Fig. 9d. The projected average monthly streamflow is higher than the baseline period from January to December by MRI-CGCM3, INMCM-4, and ensemble mean. In the near future, the highest streamflow is observed in the rainy season (June, July, August and September) while the lowest is observed in the summer season (March, April and May) by the INMCM-4, MRI-CGCM3 and ensemble mean. During the rainy season, the lowest and highest streamflow changes range from about 631.07–2718.42 m^3/s by INMCM-4, 491.71–2938 m^3/s by MRI-CGCM3 and 513.02–2270.18 m^3/s by ensemble mean, in the near future. Similarly, during summer season, the lowest level of stream flow, 158.27 m^3/s observed by MRI-CGCM3, 193.38 m^3/s (ensemble mean) and 258.53 m^3/s (INMCM-4), respectively.

6 Monthly and Seasonal Variation

Non-parametric Mann–Kendall (MK) and Sen’s slope trend tests are analyzed, and the streamflow data of INMCM-4, MRI-CGCM3 and ensemble mean at monthly, seasonal and annual scale during the time period from 2011–2040 are shown in Table 5. In this table, a

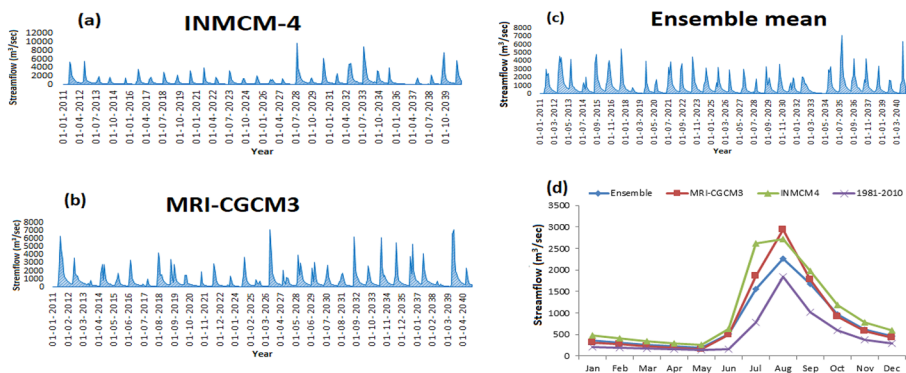


Fig. 9 Streamflow projections based on the NEX-GDDP-CMIP5 datasets, during the period of 2011–2040 (a)–(c) and (d) mean monthly streamflow using the NEX-GDDP-CMIP5 v/s IMD datasets

Table 5 MK trend test statistics of streamflow during time period 2011–2040 under the Ensemble mean, MRI-CGCM3 and INMCM-4 model

Month	Ensemble mean			INMCM-4			MRI-CGCM3		
	z	p	Slope	z	p	Slope	z	p	Slope
Jan	−0.24	0.80	−1.07	0.35	0.72	2.12	1.21	0.22	6.48
Feb	0.32	0.67	−0.04	0.38	0.68	1.14	1.35	0.17	5.44
March	−0.14	0.88	−0.84	0.42	0.52	1.53	1.35	0.17	5.44
April	−0.21	0.83	−0.84	0.39	0.69	1.22	1.39	0.16	3.61
May	−0.28	0.77	−0.92	0.21	0.83	0.48	1.10	0.26	2.79
June	1.42	0.15	0.13	0.17	0.42	0.23	0.41	0.25	0.97
July	1.78	0.07	0.41	−0.10	0.34	−0.61	−0.64	0.22	−0.9
Aug	1.21	0.22	0.21	0.82	0.11	0.32	0.17	1.08	1.11
Sep	0.43	0.31	0.03	0.21	0.57	0.45	0.46	0.26	0.14
Oct	0.07	0.94	2.73	−0.67	0.49	−9.47	−0.46	0.46	−4.68
Nov	0.03	0.97	0.40	0.39	0.69	2.73	0.21	0.83	1.75
Dec	−0.42	0.66	−1.26	0.35	0.72	2.77	0.42	0.66	2.76
Pre-monsoon	−0.17	0.85	−0.66	−0.32	0.74	−1.04	−1.28	0.19	−3.27
South-west monsoon	1.14	0.25	2.86	0.49	0.61	1.92	1.07	0.28	25.53
Winter monsoon	0.14	0.88	0.97	0.35	0.72	1.95	1.21	0.22	6.75
Post-monsoon	−0.54	1.33	−0.93	−0.71	0.47	−5.15	−0.17	0.85	−1.89

positive standard normal variate (Z) and probability (P) indicate the ascending trend, while a negative Z and P value represents a descending trend. Obtained results show the non-significant ascending and the decreasing trend observed by the individual and ensemble mean at the 95% significant level. At the monthly scale, the descending trend is observed in July and October, while other months show the ascending trend under the INMCM-4, MRI-CGCM3 model. On the other hand, a descending trend is observed in the month of January, March and December and the rest of the months show ascending trend under the ensemble mean model. The seasonal scale shows an ascending trend, which is observed in the South-west monsoon and Winter monsoon alternately; descending trend is detected in Pre-monsoon and Post-monsoon seasons of INMCM-4, MRI-CGCM3 and ensemble mean.

7 Conclusions

This study represented an approach that integrated climate data with a SWAT model to evaluate the streamflow component to projected climate change in a basin. The climate model output from the NEX-GDDP-CMIP5 under the RCP4.5 scenarios was used in order to assess the performance over the study region. An analysis of climate projections indicated that output from INMCM-4, MRI-CGCM3 and ensemble mean performed the

best among the six selected models over the MRB. The result depicted that precipitation peaked in August and September while the frequency of extreme temperature (maximum and minimum) increases over all months in the near future of INMCM-4, MRI-CGCM3 and ensemble mean. Further, the SWAT model has been calibrated and validated using observed datasets. This modelling study reveals that annual average streamflow will be increased by 76.74% ($1031.24 \text{ m}^3/\text{sec}$) based on the INMCM-4 outputs, 25% ($778.71 \text{ m}^3/\text{sec}$) based on the MRI-CGCM3 outputs, and 24.53% ($773.11 \text{ m}^3/\text{sec}$) based on the ensemble mean in the near future.

Further, the percentage change in high and low streamflow with respect to the baseline time period and the difference between the high and low streamflow would be increasing in the near future. Thus, it can be illustrated that low streamflow is observed during the summer season, which causes water shortage, drought and high flow during the rainy season, leading to floods and other water-related disasters. Similar trends are observed on monthly and seasonal flows under the INMCM-4, MRI-CGCM3, and ensemble mean. Thus, results from this study provide a better understating of streamflow of river basins. This could be useful for the scientific communities, researchers as well as decision makers to develop climate change adaptation strategies for planning and managing the water resource in the basin.

Acknowledgements The first author is thankful to the University Grant Commission and DST-Mahamana Centre of Excellence in Climate Change Research, Banaras Hindu University for providing the research fellowship for this study.

Author Contributions Conceptualization, PKS; methodology, PKS, SM; software, SM; validation, SM and LZ; formal analysis, SM and AY; investigation, SM; resources, PKS and RKM; data curation, AY and SM; writing—original draft preparation, SM and AY; writing—review and editing- SM, PKS, AY, RKM, LZ; visualization, SM and AY; supervision, PKS.; project administration, PKS and RKM; funding acquisition, PKS and RKM.

Availability of Data and Materials CMIP5 datasets used in this study are freely available and ground discharge datasets can be obtained after requesting to the Central Water Commission, India.

Declarations

Ethical Approval This Research involve No Human Participants and/or Animals and complied with ethical standards. There is no potential conflict of interests.

Consent to Participate and Publish All authors have read and agreed to the current version of the manuscript and provided consent to participate.

Competing Interest The authors declare no competing interests.

References

- Abbaspour KC, Johnson C, Van Genuchten MT (2004) Estimating uncertain flow and transport parameters using a sequential uncertainty fitting procedure. *Vadose Zone J* 3:1340–1352
- Abbaspour KC, Yang J, Maximov I, Siber R, Bogner K, Mieleitner J, Zobrist J, Srinivasan R (2007) Modelling hydrology and water quality in the pre-alpine/alpine Thur watershed using SWAT. *J Hydrol* 333:413–430
- Ahsan M, Shakir A, Zafar S, Nabi G, Ahsan E (2016) Assessment of climate change and variability in temperature, precipitation and flows in Upper Indus Basin. *Int J Sci Eng Res* 7:1610–1620

- Arnold J, Allen P (1996) Estimating hydrologic budgets for three Illinois watersheds. *J Hydrol* 176:57–77
- Arnold JG, Srinivasan R, Muttiah RS, Williams JR (1998) Large area hydrologic modeling and assessment part I: model development I. *JAWRA J Am Water Resour Assoc* 34:73–89
- Barthel R, Janisch S, Nickel D, Trifkovic A, Hörhan T (2010) Using the multiactor-approach in Głowa-Danube to simulate decisions for the water supply sector under conditions of global climate change. *Water Resour Manag* 24:239–275
- Basha G, Kishore P, Ratnam MV, Jayaraman A, Kouchak AA, Ouarda TB, Velicogna I (2017) Historical and projected surface temperature over India during the 20th and 21st century. *Sci Rep* 7:1–10
- Bermúdez M, Cea L, Van Uytven E, Willems P, Farfán J, Puertas J (2020) A robust method to update local river inundation maps using global climate model output and weather typing based statistical downscaling. *Water Resour Manag* 34:4345–4362
- Bhati DS, Dubey SK, Sharma D (2021) Application of satellite-based and observed precipitation datasets for hydrological simulation in the Upper Mahi River Basin of Rajasthan, India. *Sustainability* 13:7560
- Bhatta B, Shrestha S, Shrestha PK, Talchabhadel R (2019) Evaluation and application of a SWAT model to assess the climate change impact on the hydrology of the Himalayan River Basin. *CATENA* 181:104082
- Bird KJ, Charpentier RR, Gautier DL (2008) Circum-arctic resource appraisal: Estimates of undiscovered oil and gas north of the arctic circle. USGS
- Chaturvedi RK, Joshi J, Jayaraman M, Bala G, Ravindranath N (2012) Multi-model climate change projections for India under representative concentration pathways. *Curr Sci* 791–802
- Das S, Scaringi G (2021) River flooding in a changing climate: rainfall-discharge trends, controlling factors, and susceptibility mapping for the Mahi catchment, Western India. *Nat Hazards* 109:2439–2459
- Islam A, Sikka AK, Saha B, Singh A (2012) Streamflow response to climate change in the Brahmani River Basin, India. *Water Resour Manag* 26:1409–1424
- Jain S, Salunke P, Mishra SK, Sahany S, Choudhary N (2019) Advantage of NEX-GDDP over CMIP5 and CORDEX data: Indian summer monsoon. *Atmos Res* 228:152–160
- Ji G, Lai Z, Xia H, Liu H, Wang Z (2021) Future runoff variation and flood disaster prediction of the yellow river basin based on CA-markov and SWAT. *Land* 10:421
- Kumar N, Singh SK, Srivastava PK, Narsimlu B (2017) SWAT Model calibration and uncertainty analysis for streamflow prediction of the Tons River Basin, India, using Sequential Uncertainty Fitting (SUFI-2) algorithm. *Model Earth Syst Environ* 3:30
- Kumar P, Kumar S, Barat A, Sarthi PP, Sinha AK (2020) Evaluation of NASA's NEX-GDDP-simulated summer monsoon rainfall over homogeneous monsoon regions of India. *Theoret Appl Climatol* 141:525–536
- Lenhart T, Eckhardt K, Fohrer N, Frede H-G (2002) Comparison of two different approaches of sensitivity analysis. *Phys Chem Earth Parts a/b/c* 27:645–654
- Li L, Yang J, Wu J (2020) Future flood risk assessment under the effects of land use and climate change in the tiaoxi basin. *Sensors* 20:6079
- Maurya S, Srivastava PK, Yaduvanshi A, Anand A, Petropoulos GP, Zhuo L, Mall R (2021) Soil erosion in future scenario using CMIP5 models and earth observation datasets. *J Hydrol* 594:125851
- Mishra V, Kumar D, Ganguly AR, Sanjay J, Mujumdar M, Krishnan R, Shah RD (2014) Reliability of regional and global climate models to simulate precipitation extremes over India. *J Geophys Res Atmos* 119:9301–9323
- Moriasi DN, Gitau MW, Pai N, Daggupati P (2015) Hydrologic and water quality models: Performance measures and evaluation criteria. *Trans ASABE* 58:1763–1785
- Musie M, Sen S, Srivastava P (2020) Application of CORDEX-AFRICA and NEX-GDDP datasets for hydrologic projections under climate change in Lake Ziway sub-basin, Ethiopia. *J Hydrol Reg Stud* 31:100721
- Narsimlu B, Gosain AK, Chahar BR (2013) Assessment of future climate change impacts on water resources of Upper Sind River Basin, India using SWAT model. *Water Resour Manag* 27:3647–3662
- Narsimlu B, Gosain AK, Chahar BR, Singh SK, Srivastava PK (2015) SWAT model calibration and uncertainty analysis for streamflow prediction in the Kunwari River Basin, India, using sequential uncertainty fitting. *Environ Process* 2:79–95
- Nash JE, Sutcliffe JV (1970) River flow forecasting through conceptual models part I—A discussion of principles. *J Hydrol* 10:282–290

- Oo HT, Zin WW, Kyi CT (2020) Analysis of streamflow response to changing climate conditions using SWAT model. *Civil Eng J* 6:194–209
- Pai D, Sridhar L, Rajeevan M, Sreejith O, Satbhai N, Mukhopadhyay B (2014) Development of a new high spatial resolution (0.25× 0.25) long period (1901–2010) daily gridded rainfall data set over India and its comparison with existing data sets over the region. *Mausam* 65:1–18
- Parth Sarthi P, Kumar P, Ghosh S (2016) Possible future rainfall over Gangetic Plains (GP), India, in multi-model simulations of CMIP3 and CMIP5. *Theoret Appl Climatol* 124:691–701
- Pawar U, Hire P (2018) Flood frequency analysis of the Mahi Basin by using Log Pearson Type III probability distribution. *Hydrospatial Analysis* 2:102–112
- Raghavan SV, Hur J, Liong S-Y (2018) Evaluations of NASA NEX-GDDP data over Southeast Asia: present and future climates. *Clim Change* 148:503–518
- Sabzevari AA, Zarenistanak M, Tabari H, Moghimi S (2015) Evaluation of precipitation and river discharge variations over southwestern Iran during recent decades. *J Earth Syst Sci* 124:335–352
- Saha S, Moorthi S, Pan H-L, Wu X, Wang J, Nadiga S, Tripp P, Kistler R, Woollen J, Behringer D (2010) The NCEP climate forecast system reanalysis. *Bull Am Meteor Soc* 91:1015–1058
- Sahany S, Mishra SK, Salunke P (2019) Historical simulations and climate change projections over India by NCAR CCSM4: CMIP5 vs. NEX-GDDP. *Theor Appl Climatol* 135:1423–1433
- Sahu M, Lahari S, Gosain A, Ohri A (2016) Hydrological modeling of Mahi basin using SWAT. *J Water Resour Hydraul Eng* 5:68–79
- Santhi C, Arnold JG, Williams JR, Dugas WA, Srinivasan R, Hauck LM (2001) Validation of the swat model on a large river basin with point and nonpoint sources 1. *JAWRA J Am Water Resour Assoc* 37:1169–1188
- Sarthi PP, Ghosh S, Kumar P (2015) Possible future projection of Indian Summer Monsoon Rainfall (ISMR) with the evaluation of model performance in Coupled Model Inter-comparison Project Phase 5 (CMIP5). *Global Planet Change* 129:92–106
- Sridhar A (2009) Evidence of a late-medieval mega flood event in the upper reaches of the Mahi River basin, Gujarat. *Curr Sci* 1517–1520
- Sunde MG, He HS, Hubbart JA, Urban MA (2017) Integrating downscaled CMIP5 data with a physically based hydrologic model to estimate potential climate change impacts on streamflow processes in a mixed-use watershed. *Hydrol Process* 31:1790–1803
- Thampi SG, Raneesh KY, Surya T (2010) Influence of scale on SWAT model calibration for streamflow in a river basin in the humid tropics. *Water Resour Manag* 24:4567–4578
- Touseef M, Chen L, Masud T, Khan A, Yang K, Shahzad A, Wajid Ijaz M, Wang Y (2020) Assessment of the future climate change projections on streamflow hydrology and water availability over Upper Xijiang River Basin, China. *Appl Sci* 10:3671
- Uniyal B, Jha MK, Verma AK (2015) Assessing climate change impact on water balance components of a river basin using SWAT model. *Water Resour Manag* 29:4767–4785
- Usman M, Ndehedehe CE, Manzanar R, Ahmad B, Adeyeri OE (2021) Impacts of climate change on the hydrometeorological characteristics of the soan river basin, Pakistan. *Atmosphere* 12:792
- Veijalainen N, Dubrovin T, Marttunen M, Vehviläinen B (2010) Climate change impacts on water resources and lake regulation in the Vuoksi watershed in Finland. *Water Resour Manag* 24:3437–3459
- Xu Z, Li Y, Huang G, Wang S, Liu Y (2021) A multi-scenario ensemble streamflow forecast method for Amu Darya River Basin under considering climate and land-use changes. *J Hydrol* 598:126276
- Yaduvanshi A, Bendapudi R, Nkemelang T, New M (2021) Temperature and rainfall extremes change under current and future warming global warming levels across Indian climate zones. *Weather Clim Extremes* 31:100291
- Yaduvanshi A, Sharma RK, Kar SC, Sinha AK (2018) Rainfall–runoff simulations of extreme monsoon rainfall events in a tropical river basin of India. *Nat Hazards* 90:843–861

Publisher's Note Springer Nature remains neutral with regard to jurisdictional claims in published maps and institutional affiliations.

Springer Nature or its licensor (e.g. a society or other partner) holds exclusive rights to this article under a publishing agreement with the author(s) or other rightsholder(s); author self-archiving of the accepted manuscript version of this article is solely governed by the terms of such publishing agreement and applicable law.

Authors and Affiliations

Swati Maurya^{1,2} · Prashant K. Srivastava^{1,2}  · Lu Zhuo³ · Aradhana Yaduvanshi⁴ · R. K. Mall²

✉ Prashant K. Srivastava
prashant.iesd@bhu.ac.in

Swati Maurya
mauryaswati35@gmail.com

Lu Zhuo
ZhuoL@cardiff.ac.uk

Aradhana Yaduvanshi
aradhanayaduvanshi10@gmail.com

R. K. Mall
rkmall@bhu.ac.in

¹ Remote Sensing Laboratory, Institute of Environment and Sustainable Development, Banaras Hindu University, Varanasi 221005, India

² DST-Mahamana Centre of Excellence in Climate Change Research, Institute of Environment and Sustainable Development, Banaras Hindu University, Varanasi 221005, India

³ School of Earth and Environmental Sciences, Cardiff University, Cardiff, UK

⁴ Department of Civil Engineering, Indian Institute of Technology Bombay, Powai 400076, India